

Article

Rationale for Processing of a Mg-Zn-Ca Alloy by Equal-Channel Angular Pressing for Use in Biodegradable Implants for Osteoreconstruction

Natalia S. Martynenko ¹, Natalia Yu. Anisimova ^{2,3} , Olga V. Rybalchenko ¹ , Mikhail V. Kiselevskiy ^{2,3}, Georgy Rybalchenko ⁴, Boris Straumal ^{3,5,6,*}, Diana Temralieva ^{1,3}, Almagul T. Mansharipova ⁷, Aigul O. Kabiyeva ⁸, Maratbek T. Gabdullin ⁹, Sergey Dobatkin ^{1,3} and Yuri Estrin ^{10,11} 

- ¹ A.A. Baikov Institute of Metallurgy and Materials Science of the RAS, 119334 Moscow, Russia; nataliasmartynenko@gmail.com (N.S.M.); rybalch@mail.ru (O.V.R.); diana4-64@mail.ru (D.T.); dobatkin.sergey@gmail.com (S.D.)
 - ² N.N. Blokhin National Medical Research Center of Oncology of the Ministry of Health of the Russian Federation (N.N. Blokhin NMRCO), 115478 Moscow, Russia; n_anisimova@list.ru (N.Y.A.); kisele@inbox.ru (M.V.K.)
 - ³ College of New Materials and Nanotechnologies, National University of Science and Technology "MISIS", 119071 Moscow, Russia
 - ⁴ P.N. Lebedev Physical Institute of the RAS, 142432 Moscow, Russia; rybalchenkov@lebedev.ru
 - ⁵ Institute of Nanotechnology, Karlsruhe Institute of Technology, Hermann-von-Helmholtz-Platz 1, 76344 Eggenstein-Leopoldshafen, Germany
 - ⁶ Osipyan Institute of Solid State Physics and Chernogolovka Scientific Center of the Russian Academy of Sciences, 142432 Chernogolovka, Russia
 - ⁷ Faculty of General Medicine, College of New Materials and Nanotechnologies, Kazakh-Russian Medical University, Almaty 050000, Kazakhstan; dralma@mail.ru
 - ⁸ Association of Early Career Doctors of Almaty, Almaty 050000, Kazakhstan; kabiyeva.20011@yandex.ru
 - ⁹ Institute of Engineering and Information Technologies, Kazakh British Technical University, Almaty 050000, Kazakhstan; m.gabdullin@kbtu.kz
 - ¹⁰ Department of Materials Science and Engineering, Monash University, Clayton 3800, Australia; yuri.estrin@monash.edu
 - ¹¹ Department of Mechanical Engineering, The University of Western Australia, Nedlands 6009, Australia
- * Correspondence: boris.straumal@kit.edu



Citation: Martynenko, N.S.; Anisimova, N.Y.; Rybalchenko, O.V.; Kiselevskiy, M.V.; Rybalchenko, G.; Straumal, B.; Temralieva, D.; Mansharipova, A.T.; Kabiyeva, A.O.; Gabdullin, M.T.; et al. Rationale for Processing of a Mg-Zn-Ca Alloy by Equal-Channel Angular Pressing for Use in Biodegradable Implants for Osteoreconstruction. *Crystals* **2021**, *11*, 1381. <https://doi.org/10.3390/cryst11111381>

Academic Editors: Hongbin Bei, Björn Wiese, Mert Celikin and Chamini L. Mendis

Received: 22 October 2021
Accepted: 10 November 2021
Published: 12 November 2021

Publisher's Note: MDPI stays neutral with regard to jurisdictional claims in published maps and institutional affiliations.



Copyright: © 2021 by the authors. Licensee MDPI, Basel, Switzerland. This article is an open access article distributed under the terms and conditions of the Creative Commons Attribution (CC BY) license (<https://creativecommons.org/licenses/by/4.0/>).

Abstract: Widespread use of Mg-Zn-Ca alloys in clinical orthopedic practice requires improvement of their mechanical properties—in particular, ductility—and enhancement of their bioactivity for accelerated osteoreconstruction. The alloy was studied in two structural states: after homogenization and after equal-channel angular pressing. Immersion and potentiodynamic polarization tests showed that the corrosion rate of the alloy was not increased by deformation. The mass loss in vivo was also statistically insignificant. Furthermore, it was found that deformation did not compromise the biocompatibility of the alloy and did not have any significant effect on cell adhesion and proliferation. However, an extract of the alloy promoted the alkaline phosphatase activity of human mesenchymal stromal cells, which indicates osteogenic stimulation of cells. The osteoinduction of the deformed alloy significantly exceeded that of the homogenized one. Based on the results of this work, it can be concluded that the alloy Mg-1%Zn-0.3%Ca modified by equal-channel angular pressing is a promising candidate for the manufacture of biodegradable orthopedic implants since it stimulates osteogenic differentiation and has greater ductility, which provides it with a competitive advantage in comparison with the homogenized state.

Keywords: magnesium alloy; equal-channel angular pressing; biodegradation; biocompatibility; alkaline phosphatase activity; osteoconduction

1. Introduction

Magnesium and its alloys are considered as potential candidates for orthopedic implants that can replace permanent metal implants based on titanium or stainless steel. The

advantage of Mg alloys is their biodegradability and osteoconduction, in combination with sufficiently good mechanical properties [1,2]. In contrast with titanium or steel implants, magnesium alloys do not cause stress-shielding issues and are characterized by greater mechanical stability than polymer materials [3]. Mg-based alloys are also bioactive, exhibiting antibacterial and antitumor effects [4]. In addition, the alkaline medium formed during the destruction of Mg alloys shows bactericidal activity [5] and has been demonstrated to have a cytotoxic effect on tumor cells [6–8]. The bactericidal properties of Mg-based alloys can reduce the risk of inflammation after implantation, and the higher sensitivity of tumor cells to the degradation products of Mg alloys in comparison with non-transformed cells can lead to the elimination of residual tumor cells after bone resection in patients with osteosarcoma [9,10]. However, the excessively high biocorrosion rate of Mg-based alloys prevents their introduction in clinical practice as implants and bone-fixation elements. The problem is compounded by the release of hydrogen gas associated with the biocorrosion, which can have a cytotoxic effect on the tissues adjacent to the implant [11,12]. Alloying with various elements is commonly practiced to improve the mechanical properties and reduce the rate of degradation of pure magnesium [13]. Zn [14], Mn [15], Ca [16], and Sr [17], as well as other rare earth elements [18], are most often used in magnesium alloys. Not only do these elements have a positive effect on mechanical properties and corrosion resistance, but they also have good biocompatibility [19]. For example, alloying magnesium with calcium changes its mechanical properties and enables an increase in its biocompatibility and osteoconductivity. However, the insufficient mechanical performance and low corrosion resistance of binary Mg-Ca alloys are a significant disadvantage [20]. Recently, zinc and its alloys were used for the development of bone implants [21]. This was motivated by the favorable effect of Zn ions on bone growth and mineralization [22]. In addition, Zn has great potential as an alloying element in terms of improving the mechanical properties and corrosion resistance of Mg-based alloys [23]. The addition of Zn to magnesium alloys reduces their grain size, increases corrosion resistance, and improves tensile strength and tensile-creep properties [24,25]. On the other hand, the addition of Ca to binary Mg-Zn alloys boosts their bioactivity [26]. Owing to a set of desirable properties, including biocompatibility, biodegradability, and mechanical characteristics similar to those of human bone, alloys of the Mg-Zn-Ca system are gaining popularity as candidate materials for biomedical implants, especially for bone restoration, [27]. However, increasing the Ca content may compromise the corrosion resistance of a magnesium alloy because of the acceleration of microgalvanic corrosion. Recent studies showed that Mg-3Zn-0.2Ca alloy exhibits a good combination of mechanical properties and corrosion resistance with a high level of biocompatibility both *in vitro* and *in vivo* [28–30]. It was found that an optimal Ca content in a Mg alloy is in the range of 0.5–1.0 wt.%, while further increase in its content raises the biocorrosion rate of the alloy [31]. Zhang et al. [32] studied plates made from Mg-2 wt.% Zn-0.5 wt.% Ca (ZC21) and showed that the biodegradation rate of the alloy was sufficiently low for the intended application as an implant material. Furthermore, the alloy exhibited a good compatibility with mesenchymal stem cells of the bone marrow. All this suggests that a study of alloys of the Mg-Zn-Ca system as potential candidates for medical implants (screws, plates, staples, etc.) is worthwhile. Specifically, it is necessary to be able to vary the mechanical-property profile of the alloys depending on the targeted application. For example, a material for screws and plates must have a high strength (including fatigue strength), while a primary requirement of materials for staples is high ductility. Therefore, the study of the ways in which the mechanical properties of magnesium alloys intended for medical applications can be modified in a controlled way is an important part of implant development.

This article is devoted to assessing the effect of equal-channel angular pressing (ECAP) [33,34] on the biodegradation rate and biocompatibility *in vitro* and *in vivo* of the alloy Mg-1%Zn-0.3%Ca. It is known that ECAP can significantly improve the mechanical and in-service properties of metallic materials [35–37]. In the case of magnesium alloys, ECAP makes it possible to improve their strength [38] and, in addition, increase

ductility due to the ECAP-induced transformation of texture [39,40]. In the past, we studied the effect of ECAP on the mechanical properties of alloy Mg-1%Zn-0.3%Ca [41]. It was shown in that study that ECAP leads to a slight increase in strength (including the fatigue strength), the main effect being doubling of ductility. Such an increase in ductility qualifies the alloy as a material for manufacturing staples for fixation of bone fractures, provided that other performance requirements are satisfied. Therefore, in the present work, we concentrated on the effect of ECAP on the biodegradation rate, osteoinduction *in vitro*, and biocompatibility (both *in vitro* and *in vivo*) of the alloy Mg-1.0%Zn-0.3%Ca.

2. Materials and Methods

2.1. Material Investigated

Mg (99.95%), Ca (99.5%), and Zn (99.99%) were used for alloy smelting. Smelting was carried out in a graphite crucible in a protective atmosphere (Ar + 1 vol.% SF₆) at 750 °C and poured into a graphite mold. The cast alloy Mg-1.0%Zn-0.3%Ca was treated thermomechanically according to the following schedule: annealing at 350 °C for 12 h, followed by annealing at 450 °C for 8 h. After this thermal treatment, the material was extruded at 300 °C with an extrusion ratio of 36 and extrusion rate 0.3 s⁻¹ to obtain billets of the required shape and size. After extrusion, the alloy was annealed again at 450 °C for 3 h; it was then water quenched to fix the high-temperature state. Henceforth, this state will be referred to as homogenized, and the material will be designated as Mg-Zn-Ca Hom. ECAP (route Bc, die angle 120°) was carried out with a decrease in the deformation temperature from 400 to 300 °C in steps of 25 °C and with two passes at each temperature. The total number of passes was 10, which corresponds to a true strain of 8.7. This state will be referred to as Mg-Zn-Ca ECAP.

The average grain size was 106 ± 2.05 µm in the homogenized state of the alloy. ECAP led to the formation of a rather inhomogeneous microstructure, which contains both grains elongated in the direction of deformation (~20 µm wide and ~50 µm long) and small recrystallized grains (~1–3 µm). In this case, the average grain size of the alloy Mg-Zn-Ca ECAP is 4.0 ± 0.19 µm and 8.0 ± 0.18 µm in the transverse and longitudinal sections, respectively [41]. The formation of this structure led to a slight increase in the strength characteristics (for both monotonic and cyclic loading). The yield stress (YS), ultimate tensile strength (UTS) and fatigue limit of the Mg-Zn-Ca Hom. alloy were 92 ± 3 MPa, 194 ± 5 MPa, and 100 MPa, respectively. These characteristics increased to 106 ± 7 MPa, 215 ± 9 MPa, and 110 MPa, respectively, after ECAP. A most striking effect was the doubling of ductility (to 23.9 ± 1.6%), as represented by tensile elongation (El), due to the formation of an inclined basal texture [41].

Samples of three types were used for further investigation. Measurements of corrosion resistance by the method of potentiodynamic polarization (PDP) were carried out on penny-shaped specimens with a diameter of 15 mm and a thickness of 2 mm. Immersion tests and studies of cells *in vitro* were carried out on samples in the form of a $\frac{1}{4}$ disk with a diameter of 10 mm and a thickness of ~2 mm. To obtain extracts, the tested alloys were incubated in a complete growth medium based on Dulbecco's Modified Eagle's Medium (DMEM) (PanEco, Moscow, Russia) containing 10% fetal bovine serum (FBS) (HyClone, Thermo Fisher, Altrincham, UK), 4 mM L-glutamine, and 1% penicillin/streptomycin (both from PanEco, Russia) for 3 days at 37 °C in an atmosphere with 5% carbon dioxide. To study the alloy *in vivo*, platelet-shaped samples 10 × 5 × 0.3 mm in size were cut from the alloy in both structural conditions. The samples were immersed for 18–20 h in 70% ethanol for sterilization and then dried in a sterile atmosphere.

2.2. Study of the Corrosion Resistance

Corrosion resistance was assessed by electrochemical (PDP tests) and chemical methods. Electrochemical studies were carried out on an SP-300 potentiostat (Bio-Logic SAS, Seyssinet-Pariset, France) at room temperature in a 0.9% NaCl solution (pH = 7). The experimental setup included a PAR flat cell (Ametek Instruments, Oak Ridge, TN, USA)

with a ‘three-electrode configuration’ (a working electrode, a saturated calomel reference electrode, and a Pt-mesh counter electrode). Scanning was carried out at a speed of 1 mV/s in a range from 150 mV below the open circuit potential to -1000 mV. The exposure time before the start of the scan, necessary for the surface to acquire a stable potential (determination of the open circuit potential), was 10 min. For each test sample, five scans were conducted. The corrosion potential and the corrosion current density were calculated using EC-Lab software (BioLogic, Seyssinet-Pariset, France) [42].

Immersion tests were carried out in FBS at 37 °C and an atmosphere with 5% CO_2 for 3, 7, and 10 days in accordance with the ASTM recommendations [43]. After the immersion, the samples were removed from the solution, washed with distilled water, and dried at room temperature. The changes in the surface morphology of the samples after immersion were characterized using a JSM-7001F (JEOL) scanning electron microscope (SEM) equipped with an EDS attachment. After immersion in FBS and removal of the corrosion products by cleaning in a mixture of Cr_2O_3 , AgNO_3 , $\text{Ba}(\text{NO}_3)_2$, and reagent water for 1 min [43], a specimen was weighed to determine the corrosion rate by the mass-loss method. The mass change was determined by weighing on a Sartorius M2P Micro Balances Pro 11 (certified by ISO 9001) (Data Weighing Systems, Inc, Wood Dale, IL, USA) with an accuracy of three digits (per mg). The corrosion rate (CR, mm/year) of the alloy was calculated according to the equation

$$\text{CR} = 8.76 \times 10^4 \times \frac{\Delta m}{A \times t \times \rho} \quad (1)$$

where Δm is the mass loss in grams, t is the immersion time in hours, A is the specimen surface area in cm^2 , and ρ is the density of the alloy in g/cm^3 .

The relative mass loss (RML) was determined according to the formula

$$\text{RML} = \frac{m_0 - m_i}{m_0} \times 100\%, \quad (2)$$

where m_0 and m_i are the initial and final mass of the sample, respectively.

2.3. Hemolysis Assay

The C57Bl/6 mouse whole blood stabilized with 60 IU/m heparin was suspended in 5 mL sterile phosphate buffered saline (PBS) and centrifuged at 1000 rpm for 5 min to isolate red blood cells (RBCs). The RBCs were further washed 3 times with 10 mL PBS and finally suspended in 50 mL PBS. An amount of 2 mL RBC suspension was added to the alloy samples (alloy-treated cells), PBS only (Control), or Triton X-100 (PanReac, AppliChem) at a concentration of 1% (Triton-X-treated cells). Every group was represented in three wells of a 24-well plate (Falcon, USA). The plate with cells and the alloy samples was incubated at 37 °C in atmosphere with 5% carbon dioxide. After 4 h, these RBS suspensions were collected from wells and centrifuged at 1000 rpm for 5 min. A total of 100 μL of the supernatant of all samples was transferred to a 96-well plate (Corning Inc., Corning, NY, USA), and the optical density (OD) was measured with the MS Multiscan plate reader (Labsystem, Thermo Scientific, Philadelphia, PA, USA) at 540 nm. The result was expressed by the hemolysis defined by the following formula:

$$\text{Hemolysis}(\%) = \frac{(\text{OD}(\text{Alloy} - \text{treated cells}) - \text{OD}(\text{Control}))}{(\text{OD}(\text{Triton} - \text{X} - \text{treated cells}) - \text{OD}(\text{Control}))} \times 100 \quad (3)$$

2.4. Cytotoxicity Test

To assess the cell-membrane integrity, the lactate dehydrogenase (LDH) release was evaluated with the Pierce LDH Cytotoxicity Assay Kit (Thermo Scientific, USA) in accordance with the manufacturer’s directions. Mononuclear leucocytes (MLs) were separated from mouse whole blood stabilized with 60 IU/m heparin. An amount of 1 mL blood of C57Bl/6 mice ($m = 22 \pm 1$ g) was diluted with an equal amount of 1X PBS. It was

then gently overlaid on Ficoll (PanEco, Russia) with minimal mixing of the two phases and centrifuged at $600\times g$ for 20 min at room temperature. After that, the ML layer was collected carefully from the plasma/Ficoll interface and washed with DMEM at $300\times g$ for 5 min twice. MLs were suspended in a complete growth medium at a concentration of 520,000 cells in 1 mL and co-incubated (volume 2 mL) with the alloys in the 24-well plates (Corning, USA) for 24 h at $37\text{ }^{\circ}\text{C}$ in an atmosphere with 5% carbon dioxide. Cells incubated in the complete growth medium without alloys under the same conditions were used as a control. At the end of incubation, the plates were gently shaken to ensure LDH was evenly distributed in the medium. Quantitative analysis was performed on the cell culture supernatant after centrifugation at $300\times g$ for 5 min. The LDH release measurements were conducted using a colorimetric method according to the manufacturer's guidelines. The absorbance was measured at the wavelength of 492 nm with a reference at 620 nm using an MS Multiscan plate reader (Thermo Scientific, USA). The cytotoxicity of the alloys was calculated as the percentage of the LDH activity of cells co-incubated with the alloys in relation to the LDH activity in Control (% of Control).

2.5. Study of Cell Adhesion and Cell Proliferation

Multipotent mesenchymal stromal cells (MMSCs) from mouse femur bone marrow were used as a cell model. MMSCs were generated as described earlier [44,45]. In short, to isolate mouse cell precursors, C57BL/6 mice ($m = 20 \pm 1\text{ g}$) were sacrificed. Femurs from mice were dissected, and the bone marrow was flushed with DMEM. Bone marrow-derived cells were seeded in a 25 cm^2 flask with the complete growth medium at a density of 4,200,000 cells/ cm^2 and incubated at $37\text{ }^{\circ}\text{C}$ in an atmosphere with 5% carbon dioxide. After 24 h, nonadherent cells were removed by washing with PBS, and a portion of fresh complete growth medium was added. The confluency of passaged cells was about 80–90%. For the experiment, cells after the 2nd passage were used. Cells were characterized by flow cytometry on a BD FACS Canto II Cells Analyser (Becton Dickinson, Franklin Lakes, NJ, USA) with the mice-specific CD105, CD90, and CD45-antibodies (all Becton Dickinson, Franklin Lakes, NJ, USA) as CD105(+) CD90(+) CD45(–) cells. A total of 20 μL of the MMSCs in the complete growth medium was seeded on alloy samples and incubated for 30 min at $37\text{ }^{\circ}\text{C}$ in an atmosphere with 5% carbon dioxide. The MMSCs seeded on the bottom of the empty wells were used as a control. Part of these alloy samples with MMSCs was used to study cell adhesion, the rest being used to study cell proliferation. In cell-adhesion tests, the alloy samples (and cells seeded on the well bottom in control) were gently washed by PBS. For study of cell proliferation, 2 mL of the complete growth medium was added to the wells with the cells seeded on alloys (and to the control wells) and incubated for 7 days at $37\text{ }^{\circ}\text{C}$ in an atmosphere with 5% carbon dioxide. The medium was changed every 2 days. The cell adhesion and cell proliferation were calculated as the percentage of the LDH activity of cells co-incubated with the alloys in relation to the LDH activity in Control (% of Control) with the Pierce LDH Cytotoxicity Assay Kit in accordance with the manufacturer's instructions.

2.6. ALP Activity Assay

For osteogenic differentiation, the MMSCs were seeded in wells of 24-well plates at a density of 600,000 cells per well and incubated in the osteogenic differentiation medium (Cyagen, Santa Clara, CA, USA) with 10% alloy extracts for 21 days at $37\text{ }^{\circ}\text{C}$ in an atmosphere with 5% carbon dioxide. The medium containing 10% alloy extracts was refreshed every 3 days. Untreated cells incubated without alloy extracts were used as a control. Alkaline phosphatase (ALP) activity was measured for a study of osteoconductivity with ALP Assay Kit (Colorimetric, Abcam, UK) following the instructions of the manufacturer. The influence of alloys on the ALP activity of the cells was evaluated as the percentage of control.

2.7. Biocompatibility In Vivo

The pre-experiment acclimatization of the mice was assured by hosting them in constant temperature (22 ± 0.7 °C) and humidity ($60 \pm 10\%$) conditions. Animal experiments were performed according to the *Guide for Care and Use of Laboratory Animals* and the European legislation on animal use. A total of 12 ten-week-old male Balb/c mice were divided into three equal groups based on implant alloy type in the host mice: control, Mg-Zn-Ca Hom. group, and Mg-Zn-Ca ECAP group. The samples were implanted subcutaneously in mice of the Mg-Zn-Ca Hom. group and Mg-Zn-Ca ECAP group. The mice of the control group were treated in the same manner as those in the other two groups without implantation of any alloy. The animals were monitored and clinically examined daily for possible disease conditions or abnormal behavior. They were sacrificed after four weeks, and implanted alloy samples were extracted for analysis of corrosion. Before the removal of the alloys, the mice were examined, and accumulation of gas was noted. The morphology of the area of implantation was inspected after the removing the implants. Signs of inflammation, necrosis, and gas accumulation were found. To identify the specific effect of the alloys, the results in the Mg-Zn-Ca Hom. and Mg-Zn-Ca ECAP groups of mice were compared with the control group. The mass change was determined by weighing of the animals on a Sartorius M2P Micro Balances Pro 11 (certified by ISO 9001) (Data Weighing Systems, Inc, Wood Dale, IL, USA) with an accuracy of three digits (per mg). The relative weight loss (RML) was determined based on Equation (2).

2.8. Ethics Statement

The animal and cell-test protocols were evaluated and approved by the Local Ethics Committee of the “N.N. Blokhin National Medical Research Center of Oncology” of the Ministry of Health of the Russian Federation (project#660, Agreement 075-15-2021-965, 24 September 2021).

2.9. Statistical Analysis

All statistical analyses were carried out using Statistica 6.0 (StatSoft, Tulsa, OK, USA). Differences among the groups were analyzed by using one-way ANOVA and student’s one-tailed *t*-test versus control. All experiments were conducted at least three times, and the data are presented as a mean \pm standard deviation (SD). Results were considered statistically significant when $p < 0.05$.

3. Results

3.1. Corrosion Resistance

Figure 1 and Table 1 show the data for the corrosion resistance of the alloy Mg-1%Zn-0.3%Ca by the PDP method.

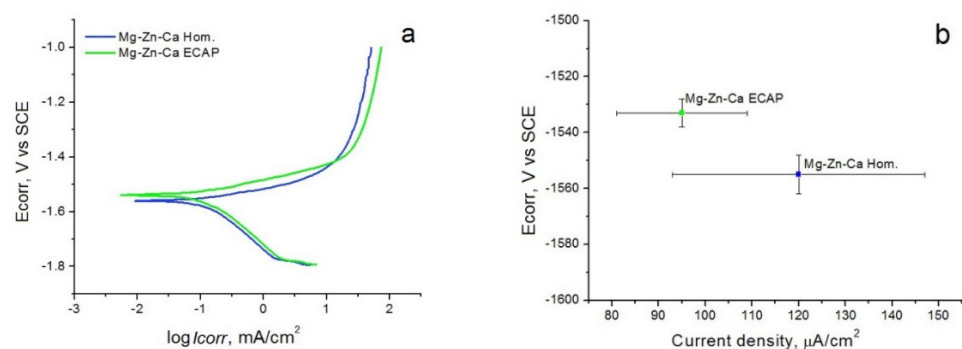


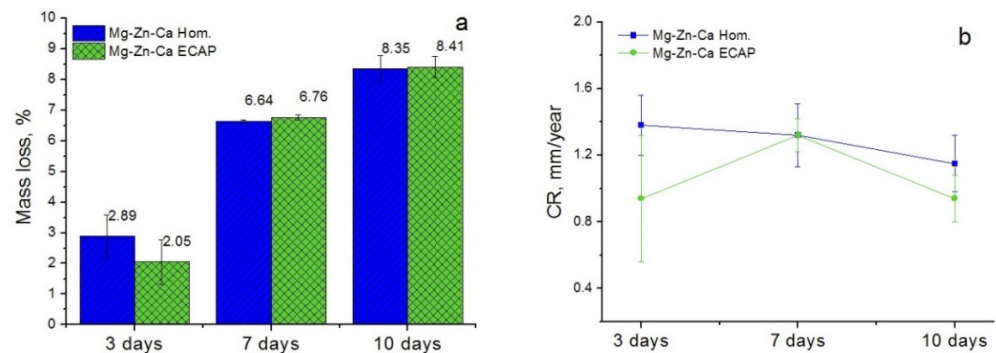
Figure 1. The results of the corrosion tests on Mg-1%Zn-0.3%Ca in the initial state and after ECAP: (a) the potential E_{corr} (in mV) with respect to a saturated calomel electrode (SCE) vs. current density; (b) comparison of the results of the potentiodynamic tests for the homogenized with the ECAP-processed specimens.

Table 1. Corrosion resistance of Mg-1%Zn-0.3%Ca measured by the PDP method (E_{corr} —corrosion potential, I_{corr} —current density).

State	E_{corr} , mV (vs SCE)	I_{corr} , $\mu\text{A}/\text{cm}^2$
Mg-Zn-Ca Hom.	-1555 ± 7	120 ± 27
Mg-Zn-Ca ECAP	-1533 ± 5	95 ± 14

The refinement of the microstructure caused by ECAP did not lead to a significant change in the parameters of electrochemical corrosion. The corrosion potential changed after ECAP to -1533 ± 5 mV, compared to -1555 ± 7 mV in the initial state, which indicates a slight increase in electrochemical corrosion resistance. At the same time, the corrosion current density remained unchanged within the experimental error (120 ± 27 and 95 ± 14 $\mu\text{A}/\text{cm}^2$ for Mg-Zn-Ca Hom., and Mg-Zn-Ca ECAP, respectively).

Figure 2 shows the data for the mass loss of the alloy before and after ECAP after its incubation in FBS for 3, 7, and 10 days. It should be noted that ECAP of the alloy Mg-1%Zn-0.3%Ca did not raise the rate of chemical corrosion over the entire period of the test. The incubation of alloy samples in both microstructural states in FBS for 10 days led to a decrease in the weight of the samples of less than 10%. The RML, after 3 days of incubation, was $2.89 \pm 0.70\%$ and $2.05 \pm 0.73\%$; after 7 days, $6.64 \pm 0.05\%$ and $6.76 \pm 0.08\%$; and after 10 days, $8.35 \pm 0.42\%$ and $8.41 \pm 0.34\%$ for Mg-Zn-Ca Hom. and Mg-Zn-Ca ECAP, respectively (Figure 3a). The calculation of CR (mm/year) using Equation (1) showed that ECAP did not have any effect on the corrosion resistance of the alloy (Figure 2b). After 3 days of incubation, CR was estimated at 1.38 ± 0.18 and 0.94 ± 0.38 mm/year; after 7 days, it was 1.32 ± 0.19 and 1.32 ± 0.10 mm/year; and after 10 days, the values dropped to 1.15 ± 0.17 and 0.94 ± 0.14 mm/year for Mg-Zn-Ca Hom. and Mg-Zn-Ca ECAP, respectively (Figure 2b). By contrast, the chemical corrosion rate remained practically unchanged throughout the whole test duration.

**Figure 2.** Mass loss of the alloy in the homogenized and ECAP conditions in vitro (a) in bar form (b) as a plot.

Figures 3 and 4 show SEM micrographs of the surface of alloy samples in both microstructural states after incubation with FBS for 10 days.

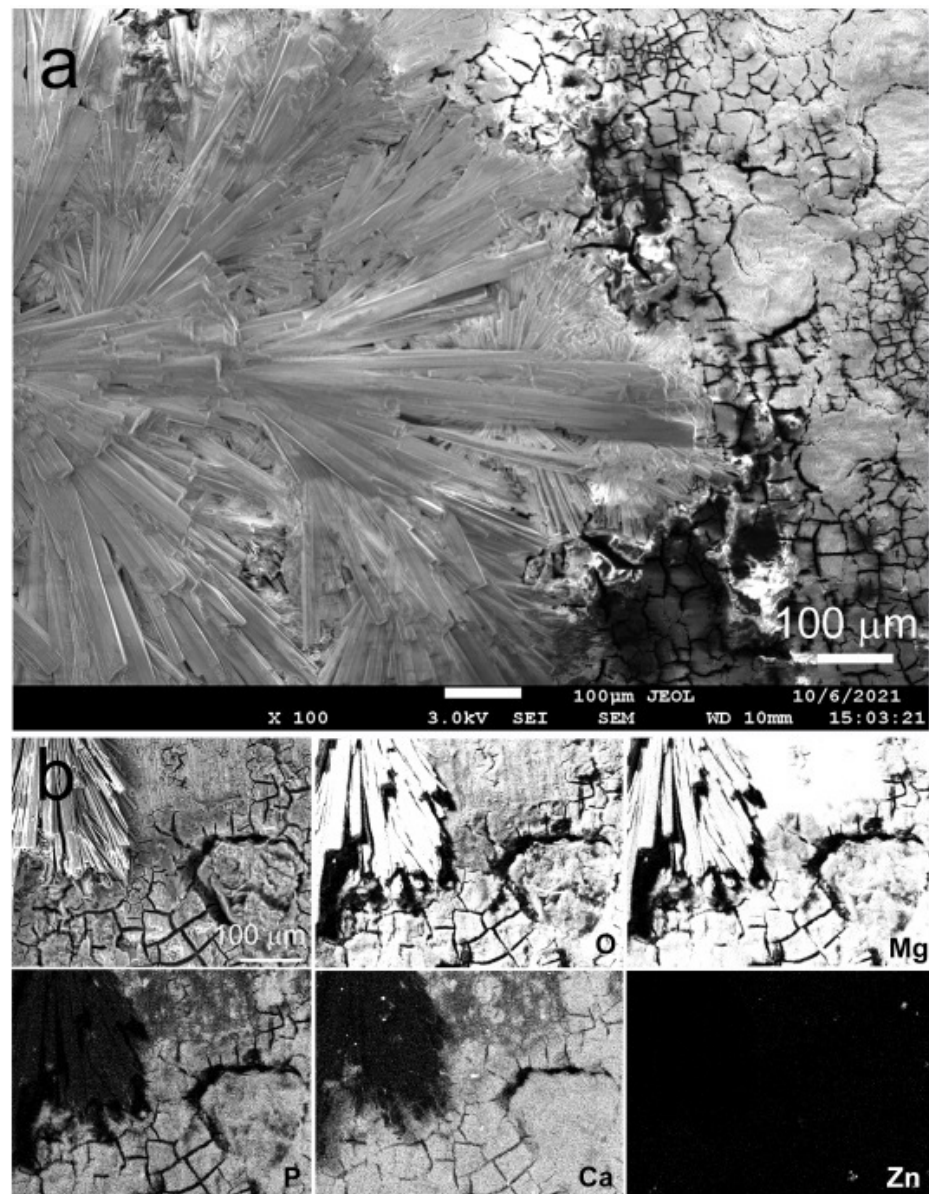


Figure 3. SEM images of corroded surfaces (a) and elemental mapping (b) of “Mg–Zn–Ca Hom.” alloy samples after incubation in FBS for 10 days.

The formation of a thick layer of degradation products and large needle-shaped crystals was observed on the surface of the Mg–Zn–Ca Hom. In this case, the layer of degradation products is rather heterogeneous, dotted with a large number of cracks, and at some places, exfoliates from the surface of the sample (Figure 3). The study of the elemental composition of degradation products showed that crystals contain mainly magnesium and oxygen. Most likely, these crystals are oxides and/or hydroxides of magnesium [19,46]. The film contains a large amount of O, Mg, P, and Ca, as well as a small amount of Zn. Zn (as well as partly Ca) was probably released from the alloy matrix. However, a large amount of Ca in the degradation products cannot be associated only with its presence in the alloy composition, as its nominal content is fairly low (0.3 wt.%). We assume that the presence of a large amount of Ca (and P) in the degradation products originated from FBS used as a corrosive medium [47].

No formation of needle-shaped crystals was detected on the surface of the Mg–Zn–Ca ECAP alloy. The surface of the samples was covered with a layer of degradation products

uniform in thickness (Figure 4). However, a large number of through-thickness cracks were observed in the surface layer. As in the case of the Mg-Zn-Ca Hom., O, Mg, P, Ca, and a small amount of Zn were prevalent in the composition of degradation products.

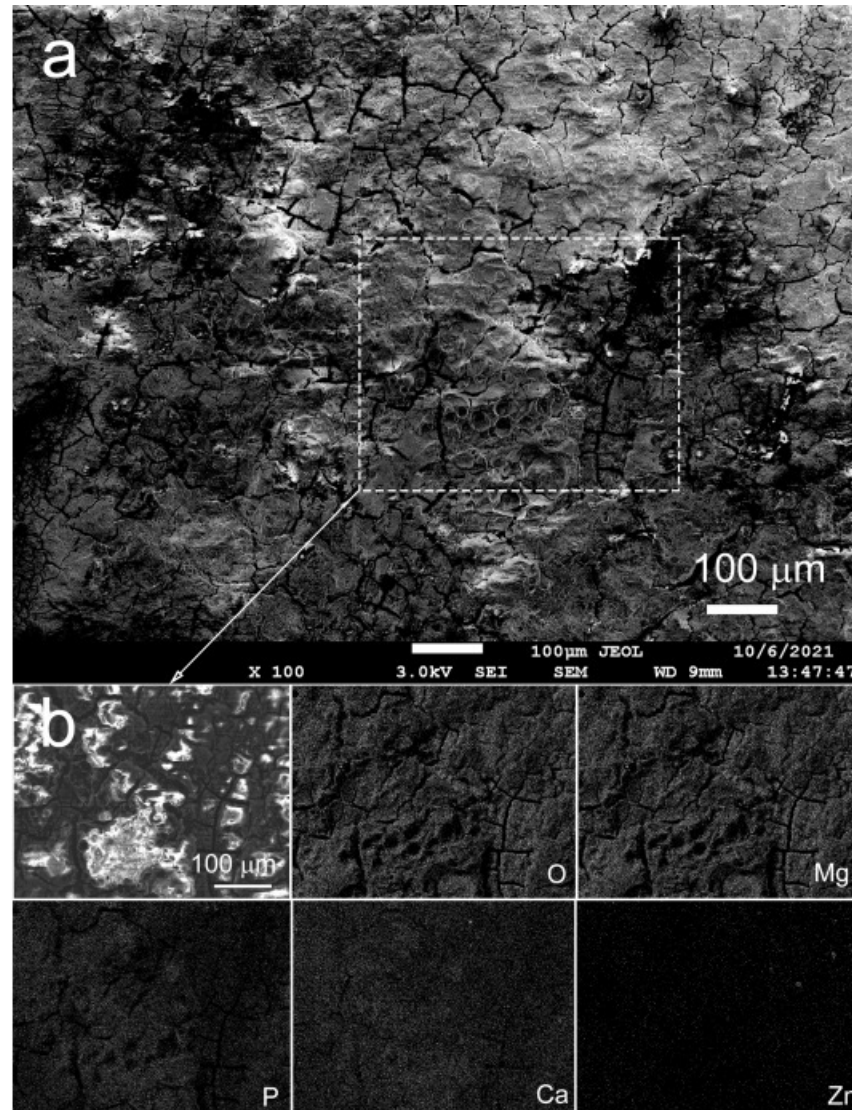


Figure 4. SEM images of corroded surfaces (a) and elemental mapping (b) of “Mg-Zn-Ca ECAP” alloy samples after incubation in FBS for 10 days.

3.2. The Study of Biocompatibility In Vitro

Since the alloy studied is intended for use in medical devices for osteoreconstruction (including bioimplants for bone replacement, pins, and fasteners), it was necessary to carry out biocompatibility testing. For this purpose, we evaluated their hemolytic activity and cytotoxicity to blood cells in vitro.

The tests showed that the hemolytic activity of both investigated types of the alloy after 4 h of incubation of RBCs on the surface of the samples was too weak for statistically confirmed hemolysis to be established (Figure 5). Similarly, there was no statistically proven cytotoxic effect of Mg-Zn-Ca alloy before and after ECAP against MLs after 1 day of their co-incubation with alloy samples. Therefore, the assessment of the specific properties of the alloy was carried out after their biocompatibility was confirmed.

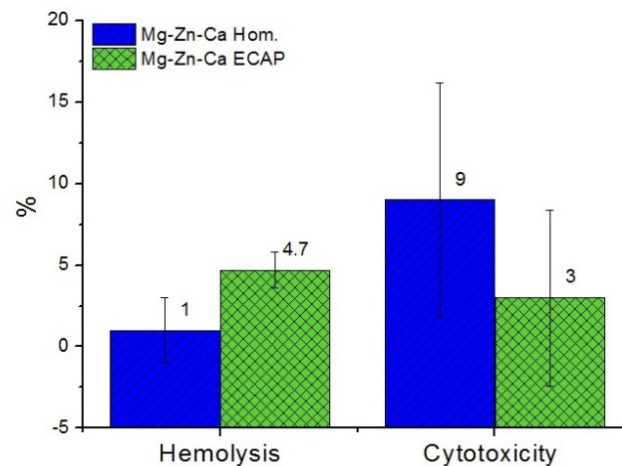


Figure 5. Biocompatibility in vitro of the alloy Mg–Zn–Ca before and after ECAP.

3.3. Stimulation of Cell Adhesion and Cell Proliferation

Osteoconduction (the ability to stimulate the adhesion of cells capable of osteogenesis) and osteoinduction (the ability to induce the differentiation of multipotent cells into osteogenic ones) are extremely important properties, which are critical when assessing their suitability as implant materials for successful osteoreconstruction. The combination of these qualities is capable of providing rapid osseointegration of the implant and the stability of osteosynthesis. In our study, MMSCs from bone marrow with osteogenic potential were used as a cellular model.

It was found that both types of the alloy stimulate cell adhesion, which may indicate osteoconductive activity (Figure 6). At the same time, long-term (two-week) incubation of MMSCs on the surface of samples demonstrated a decrease in the intensity of cell proliferation in comparison with the control group, where cells were cultured without alloy samples ($p < 0.05$). The activity of both types of the alloy differed insignificantly ($p > 0.05$). As is known, the extinction of proliferation, up to complete inhibition of mitotic activity, was preceded by beginning of the stage of MMSC differentiation. Therefore, as a next step, the osteoinductive activity of the alloys was evaluated. The activity of both types of the alloy also differed only insignificantly ($p > 0.05$).

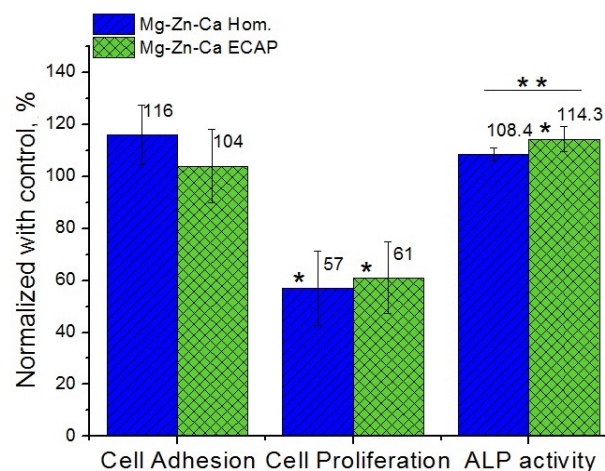


Figure 6. Osteoconduction and osteoinduction of Mg–Zn–Ca Hom. and Mg–Zn–Ca ECAP alloy: adhesion and proliferation of human mesenchymal stromal cells (MSCs) on the alloy surface and alkaline phosphatase (ALP) activity of human MMSCs under treatment with extracts of alloys. Data normalized with respect to control (without alloys or extraction medium); * $p < 0.05$ versus control; ** $p < 0.05$ in a comparison of the activity of the alloy before and after ECAP.

3.4. Osteoinductive Activity

The variation of the level of alkaline phosphatase MMSC activity after incubation in a medium with extracts of alloy samples (both homogenized and ECAP-treated) was studied to reveal the osteoinductive activity of the alloy. The tests revealed a stimulating effect of the alloy extracts on the differentiation of cells shifting it in the osteogenic direction as compared to the control (Figure 6). In particular, it was found that both types of the alloy contributed to an increase in the level of ALP activity in cell culture compared with the control, where cells were incubated in a medium without alloy extracts. The osteoinductive activity of the homogenized alloy was hardly noticeable and exceeded the value in the control by just $8 \pm 2\%$, whereas the difference in activity of the alloy after ECAP increased to $14 \pm 4\%$ ($p < 0.05$).

3.5. The Study of Biocompatibility In Vivo

The data were obtained from the results of implantation of magnesium alloy samples in mice in subcutaneous pockets. A morphological examination of the tissues in the implantation area was carried out after autopsy. Separate aspects of changes in the morphology of adjacent tissues were noted during the study. In particular, neoangiogenesis, the presence of edema, necrosis, or signs of inflammation were identified and assessed.

Animals of the two groups with implanted alloys showed a pronounced swelling in the implantation area, caused by subcutaneous gas accumulation 2 days after the operation without signs of local hyperthermia, suppuration, or ulceration (Figure 7)

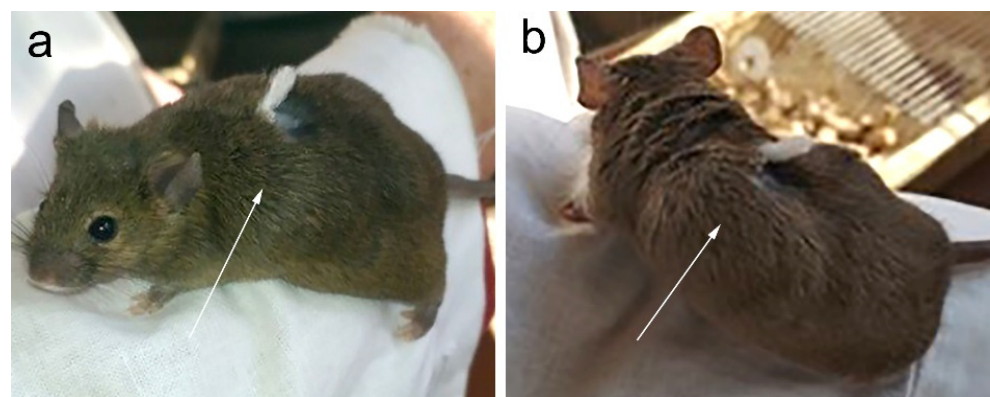


Figure 7. Accumulation of gas at the implantation site two days after surgery for: (a) Mg-Zn-Ca Hom. and (b) Mg-Zn-Ca ECAP.

Accumulation of a significant amount of gas in the subcutaneous space in the animals was observed after autopsy. This caused the appearance of a single or multiple blisters, the walls of which were formed by the subcutaneous fascia and the fascia of the latissimus dorsi (Figure 8a,b).

The examination of the tissues adjacent to the Mg-Zn-Ca implants did not reveal any signs of neoangiogenesis, accumulation of pus, blood, or edema in the alloy-tissue contact area. The entire surface of samples of both alloy types was uniformly covered with a thin capsule that did not adhere tightly to the surface of the sample (Figure 8c).

The biodegradation rate of Mg-Zn-Ca Hom. and Mg-Zn-Ca ECAP did not differ significantly during the 2 weeks of implantation in the mouse body. All samples were partially degraded, which was accompanied by the formation of fragments (1–3 mm) penetrating from the capsule around the implant into the muscle tissue. The local trauma to muscle fibers caused the appearance of small foci of hemorrhage. Fragments of samples, partially split off from the edges of the plates, were trapped in the connective tissue (Figure 8d,e).

In general, the absence of features of an acute inflammatory reaction in tissues (including rejection or inflammation) was noted.

Analyzing the results obtained, it can be concluded that contact with the studied alloy samples did not have any serious destructive effect on the adjacent tissues. However, a significant volume of gas released due to the biodegradation of the samples may have an adverse effect. Being localized in the interstitial space, a gas bubble prevents blood and lymph flow in the implantation area, putting pressure on the walls of local lymphatic and blood vessels. In addition, the change in local tissues can be associated with alkalization of the medium due to the process of biocorrosion of alloys.

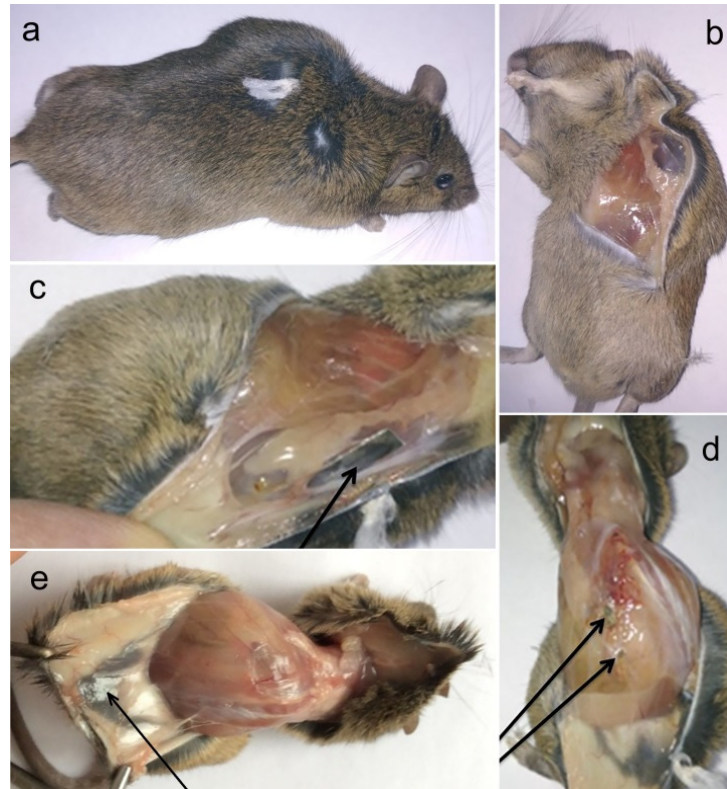


Figure 8. A gas bubble in the area of implantation of the Mg-Zn-Ca ECAP alloy 14 days after surgery: (a) appearance of the animal before autopsy; (b) gas accumulation under the skin near the implant; (c) encapsulated Mg-Zn-Ca sample; (d) intrusion of Mg-Zn-Ca biodegradation products into adjacent tissues; (e) internal tissues in contact with the sample based on the alloy Mg-Zn-Ca in vivo.

Investigation in vivo showed that ECAP had no significant effect on the biodegradation rate of the alloy Mg-1.0%Zn-0.3%Ca. The plates cut from the Mg-Zn-Ca Hom. alloy lost $19.0 \pm 1.2\%$ of their initial mass within two weeks of the start of the experiment. Similarly, the mass loss of plates cut from Mg-Zn-Ca ECAP alloy was $20.0 \pm 2.0\%$. The differences between these alloy states for the specified parameters are insignificant (on average, 1%) and unreliable ($p > 0.05$). The shape of the plates from the alloy in both microstructural states was almost completely preserved, and the structural integrity was not lost. Only slight destruction of the plates at the edges was observed. It should be noted that the higher value of the mass loss in the case of the in vivo assay, compared to that in the in vitro test, may be associated with differences in the geometry of the samples. Thin plates that fit tightly to an animal's tissue and have a large area of contact with the corrosion medium and, therefore, a large area subjected to degradation were used for the in vivo studies. The larger surface area of the samples used for implantation led to a significant increase in RML for the in vivo testing compared to the in vitro testing ($\sim 20\%$ and $\sim 8.5\%$,

respectively). A further reason for a more pronounced biodegradation in the *in vivo* case may be the dynamics of bodily fluids not replicated *in vitro*.

4. Discussion

Obviously, the material for such products should be biocompatible and have strength characteristics close to those of bone tissue. Special requirements are placed on the rate and character of the biodegradation of the alloy. The biodegradation of the implant needs to be uniform over the entire surface, which will ensure a smooth and gradual decrease in the implant's performance. In addition, it is crucial to be able to control the biodegradation rate of the implant, which is determined by the purpose of its use for treatment of a patient and the specific clinical situation. It is known that cast alloys have a non-uniform microstructure (related to the phase composition) and usually show low ductility. This limits the manufacturability of articles which require good ductility (for example, staples). Thermomechanical processing of alloys alleviates the ductility problem through modification of the microstructure. However, according to the data we obtained earlier, the surface biodegradation of samples made from homogenized alloys can be inhomogeneous enough. The result is the formation of pits and massive erosion locally, which increases the likelihood of rapid destruction of the implant [38]. In addition, we observed significant differences in the type of corrosion-induced destruction among samples obtained from a single homogenized workpiece. This causes problems with the use of such materials in medical devices since it makes it difficult to predict the time of optimal performance upon implantation. To overcome this problem while also improving the ductility, the alloy Mg-1.0%Zn-0.3%Ca was processed by ECAP. The resulting microstructure enabled a two-fold increase in the ductility of the alloy, which is an advantage in the manufacture of the final implantable articles. At the same time, the treatment of the alloy by ECAP did not seriously compromise its biodegradation rate either under *in vitro* or *in vivo* conditions. However, a significant difference in biodegradation of the alloy was observed in the morphology of the products in the two microstructural states investigated. Specifically, the formation of needle-shaped crystals of oxides/hydroxides of Mg was observed on the surface of Mg-Zn-Ca Hom. These crystals can damage the cells settled upon them and impair their proliferative properties [38]. By contrast, such crystals were not found to form in the case of the Mg-Zn-Ca ECAP alloy. The surface was covered with a loose layer of degradation products, consisting mainly of O, Mg, P, and Ca. A similar composition of degradation products was also demonstrated in earlier works [48,49].

The biocompatibility of the Mg-Zn-Ca alloy found in earlier studies [50,51] was confirmed by our results. We have shown that ECAP-induced changes in the microstructure did not worsen such biocompatibility parameters as induced hemolysis and cytotoxicity against blood cells. Biocompatibility is one of the key properties that a medical device must have to be suitable for a long-term implantation (from several months to several years) in a patient's body in close contact with surrounding tissues. The data we obtained indicate a low probability of tissue necrosis in the contact area or development of adverse reactions such as inflammation or rejection of the implant mediated by immunocompetent blood cells. The experiments *in vivo* carried out by implantation of alloy samples in mice confirmed the safety of the alloy studied, as well as the absence of acute immunological reactions at the implantation site. No signs of inflammation or rejection of implants were observed, despite a fairly rapid biodegradation of the alloy samples in the body of mice accompanied by locoregional accumulation of gases and the penetration of adjacent tissues by crystals of biodegradation products. This correlates with the results of experiments of Ding et al., who saw no tissue inflammation around the Mg-Zn-Ca clips in a rat bodies [51]. The immunological indifference of alloys used in the manufacture of products for osteoreconstruction (for example, titanium alloys) is well known. However, it is also known that many titanium-based implants do not stimulate osseointegration, i.e., integration of the implant into the patient's bone, in which a stable contact and functional connection with a load-bearing capability is formed between the implant and the bone tissue. This may cause

instability of osteosynthesis, a decrease in the functionality of the reconstructed bone, up to the loss of supporting ability of the limb and disability of the patient.

The study of the osteoconductive and osteoinductive potential of Mg-Zn-Ca alloy conducted in this work addressed the ability of Mg-Zn-Ca alloy, both before and after ECAP, to stimulate the adhesion of MMSCs, which are progenitor cells with osteogenic potential. It was found that even a short (30 min) incubation period was sufficient to fix most of the deposited cells on the surface of samples of both types of the alloy. After the cells were fixed on the surface of the samples, they proliferated, colonizing the sample surface. This occurred against the background of biodegradation, accompanied by the release of biodegradation products into the culture medium and an increase in the pH of the medium [52]. There were no statistically confirmed differences in the intensity of adhesion and proliferation of cells on the surface of samples of the alloy in the homogenized and ECAP-treated states, which indicates a weak effect of the differences in the microstructure and nature of biocorrosion of both alloys on the parameters of cellular response. Due to the work of Nakamura et al., who studied the effect of calcium ions on the behavior of osteogenic cells in vitro, it is known that an increase in calcium concentration mediates intercellular interactions and stimulates the cell-matrix contact (the cell-cell or cell-matrix interactions) [53]. Based on this, it can be concluded that one of the significant inducers of MMSC adhesion was calcium ions released during the biodegradation of samples in the growth medium. With the chemical composition of both types of the alloy being the same and their biodegradation rate not differing significantly, the difference in their microstructure did not cause any substantial differences in their cellular response.

Based on in vivo results, several researchers suggested that the use of biomedical alloys Mg-Ca and Mg-Zn-Ca for the reconstruction of bone defects is promising [54,55]. Therefore, we evaluated the osteoinduction of alloy Mg-Zn-Ca before and after ECAP for their ability to stimulate osteogenic differentiation of MMSCs in vitro in a specially designed series of experiments. According to the data obtained, the addition of extracts of both types of the alloy to the incubation medium stimulated the activity of ALP (alkaline phosphatase), a membrane protein that is a marker of osteoblasts. The activity of the alloy after ECAP was somewhat more pronounced in comparison with that of the homogenized alloy. It seems likely that this effect was achieved under the influence of alkalization of the culture medium. This assumption is based on the results of the work of Gallow et al., who studied the effect of the properties of the growth medium on the development of osteoblasts [56]. The authors concluded that elevated pH is beneficial for the cultivation of bone cells and may also provide therapeutic value in bone-regeneration therapies. The presence in the incubation medium of calcium ions released during the biodegradation of the alloy, increasing cell mineralization on the one hand and inhibiting angiogenic differentiation of MMSCs by suppressing the expression of angiopoietin-1 (angiopoietin-1) on the other hand, could also contribute to this process. Indirectly, this conclusion was confirmed by the work of Makkar et al., who found the osteoconductive and osteoinductive properties of Mg-Ca alloys and their high bone-formation capability [54], as well as by the data of Wong et al. on stimulation of differentiation of primary rabbit osteoblasts by Mg₆₀Zn₃₅Ca₅ bulk metallic glass-composite extraction medium [57]. The significance of calcium compounds for the stimulation of osteogenic differentiation of MMSCs has been studied in a number of works considering the bioactivity of calcium-containing matrices that are promising for accelerating osteosynthesis [58,59]. In our opinion, it is advisable to use a coating, for example, a calcium phosphate one, as a further means of modification of the material [60,61]. This will not only slow down the biodegradation rate in the early stages of injury healing but also stimulate the growth and proliferation of osteoblasts. The combined treatment of the alloy Mg-1%Zn-0.3%Ca involving ECAP, in conjunction with the application of special coatings, should make it possible to create implants that can perform not only the functions of bone fixators but also promote faster healing of trauma. What can be asserted already at this stage is that the use of ECAP will impart a high reserve of ductility to the alloy Mg-1%Zn-0.3%Ca, which can be used in prospective

implant applications. One specific example of such applications is braces for fixation of rib fractures; however, the pallet of potential uses of the processing route considered is certainly much broader.

5. Conclusions

The results of this study suggest that it is promising to use the Mg-1.0%Zn-0.3%Ca alloy processed by ECAP as a basis for medical devices intended for osteoreconstruction. It was found that ECAP does not cause any decrease in corrosion resistance or deterioration of the biocompatibility of the alloy in vitro and in vivo afterwards, while doubling its ductility. The biocorrosion rate did not change significantly either under in vitro or in vivo conditions. The corrosion potential was -1555 ± 7 mV and -1533 ± 5 mV, while the corrosion current density was 120 ± 27 and 95 ± 14 $\mu\text{A}/\text{cm}^2$ for Mg-Zn-Ca Hom. and Mg-Zn-Ca ECAP, respectively. The CR also did not change and was ~ 1 mm/year for alloy in both microstructural states. At the same time, the biocorrosion rate in vivo was $19.0 \pm 1.2\%$ and $20.0 \pm 2.0\%$ of initial mass of plates within two weeks of implantation for Mg-Zn-Ca Hom. and Mg-Zn-Ca ECAP, respectively. However, as distinct from the homogenized samples, no formation of needle-like crystals on the sample surface was observed, which could impair cell adhesion. It was concluded that the alloy has osteoconductive and osteoinductive properties both in the homogenized and the ECAP-treated state. However, the ECAP-processed alloy stimulates osteogenic differentiation of mesenchymal stromal cells more actively and has greater ductility, which provides it with a competitive advantage over the unprocessed alloy.

Author Contributions: Conceptualization: N.Y.A. and N.S.M.; methodology: M.V.K. and M.T.G.; software: N.Y.A., N.S.M., O.V.R. and G.R.; validation: A.T.M., A.O.K. and B.S.; formal analysis: S.D. and Y.E.; investigation: N.Y.A., N.S.M., O.V.R., D.T., M.T.G. and G.R.; resources: A.T.M., A.O.K., M.T.G. and M.V.K.; data curation: S.D., B.S. and Y.E.; writing—original draft preparation: N.Y.A. and N.S.M.; writing—review and editing: N.Y.A., N.S.M. and Y.E.; visualization: M.V.K.; supervision: S.D., M.V.K. and Y.E.; project administration: N.Y.A. and A.T.M.; funding acquisition: N.Y.A. All authors have read and agreed to the published version of the manuscript.

Funding: This work was supported by the Ministry of Science and Higher Education of the Russian Federation (Agreement No. 075-15-2021-965).

Institutional Review Board Statement: The animal and cell test protocols were evaluated and approved by the Local Ethics Committee of the “N.N. Blokhin National Medical Research Center of Oncology” of the Ministry of Health of the Russian Federation (project#660, Agreement 075-15-2021-965, 24 September 2021).

Informed Consent Statement: No humans were involved in studies.

Data Availability Statement: All the data required to reproduce these experiments are present in the article.

Acknowledgments: Our thanks go to G. Raab, who carried out the equal-channel angular pressing of the alloy used in this work. We also acknowledge the support by the KIT-Publication Fund of the Karlsruhe Institute of Technology for help in publishing this article.

Conflicts of Interest: The authors declare no conflict of interest.

References

1. Zhang, J.; Li, H.; Wang, W.; Huang, H.; Pei, J.; Qu, H.; Yuan, G.; Li, Y. The degradation and transport mechanism of a Mg-Nd-Zn-Zr stent in rabbit common carotid artery: A 20-month study. *Acta Biomater.* **2018**, *69*, 372–384. [[CrossRef](#)]
2. Rahmati, M.; Stötzel, S.; Khassawna, T.E.; Iskhahova, K.; Florian Wieland, D.C.; Zeller Plumhoff, B.; Haugen, H.J. Early osteoimmunomodulatory effects of magnesium-calcium-zinc alloys. *J. Tissue Eng.* **2021**, *22*, 1–19. [[CrossRef](#)] [[PubMed](#)]
3. Li, B.; Cao, H.; Zhao, Y.; Chen, M.; Qin, H.; Cheng, T.; Hu, Y.; Zhang, X.; Liu, X. In vitro and in vivo responses of macrophages to magnesium-doped titanium. *Sci. Rep.* **2017**, *7*, 42707. [[CrossRef](#)]
4. Lee, J.; Byun, H.; Madhurakkat Perikamana, S.K.; Lee, S.; Shin, H. Current advances in immunomodulatory biomaterials for bone regeneration. *Adv. Healthc. Mater.* **2019**, *8*, e1801106. [[CrossRef](#)] [[PubMed](#)]

5. Xie, K.; Wang, N.; Guo, Y.; Zhao, S.; Tan, J.; Wang, L.; Li, G.; Wu, J.; Yang, Y.; Xu, W.; et al. Additively manufactured biodegradable porous magnesium implants for elimination of implant-related infections: An in vitro and in vivo study. *Bioact. Mater.* **2021**, *8*, 140–152. [[CrossRef](#)]
6. Li, M.; Ren, L.; Li, L.; He, P.; Lan, G.; Zhang, Y.; Yang, K. Cytotoxic effect on osteosarcoma mg-63 cells by degradation of magnesium. *J. Mater. Sci. Technol.* **2014**, *30*, 888–893. [[CrossRef](#)]
7. Anisimova, N.; Kiselevskiy, M.; Martynenko, N.; Straumal, B.; Willumeit-Römer, R.; Dobatkin, S.; Estrin, Y. Cytotoxicity of biodegradable magnesium alloy WE43 to tumor cells in vitro: Bioresorbable implants with antitumor activity? *J. Biomed. Mater. Res. B Appl. Biomater.* **2020**, *108*, 167–173. [[CrossRef](#)] [[PubMed](#)]
8. Martynenko, N.; Anisimova, N.; Kiselevskiy, M.; Tabachkova, N.; Temralieva, D.; Prosvirnin, D.; Terentiev, V.; Koltygin, A.; Belov, V.; Morosov, M.; et al. Structure, mechanical characteristics, biodegradation, and in vitro cytotoxicity of magnesium alloy ZX11 processed by rotary swaging. *J. Magnes. Alloys* **2020**, *8*, 1038–1046. [[CrossRef](#)]
9. Fischer, J.; Pröfrock, D.; Hort, N.; Willumeit, R.; Feyerabend, F. Improved cytotoxicity testing of magnesium materials. *Mater. Sci. Eng. B* **2011**, *176*, 830–834. [[CrossRef](#)]
10. Globig, P.; Willumeit-Römer, R.; Martini, F.; Mazzoni, E.; Luthringer-Feyerabend, B.J.C. Optimizing an Osteosarcoma-Fibroblast Coculture Model to Study Antitumoral Activity of Magnesium-Based Biomaterials. *Int. J. Mol. Sci.* **2020**, *21*, 5099. [[CrossRef](#)]
11. Banerjee, P.C.; Al-Saadi, S.; Choudhary, L.; Harandi, S.E.; Singh, R. Magnesium implants: Prospects and challenges. *Materials* **2019**, *12*, 136. [[CrossRef](#)]
12. Anisimova, N.; Kiselevskiy, M.; Martynenko, N.; Willumeit-Römer, R.; Korniyushenkov, E.; Rodionov, M.; Dobatkin, S.; Estrin, Y. Anti-tumour activity of alloys Mg-6%Ag and Mg-10%Gd in two microstructural states in mice with inoculated melanoma. *Mater. Sci. Eng. C* **2021**, *130*, 112464. [[CrossRef](#)]
13. Zhang, B.; Hou, Y.; Wang, X.; Wang, Y.; Geng, L. Mechanical properties, degradation performance and cytotoxicity of Mg–Zn–Ca biomedical alloys with different compositions. *Mater. Sci. Eng. C* **2011**, *31*, 1667–1673. [[CrossRef](#)]
14. Zhang, S.; Zhang, X.; Zhao, C.; Li, J.; Song, Y.; Xie, C.; Tao, H.; Zhang, Y.; He, Y.; Jiang, Y.; et al. Research on an Mg–Zn alloy as a degradable biomaterial. *Acta Biomater.* **2010**, *6*, 626–640. [[CrossRef](#)]
15. Cho, D.H.; Lee, B.W.; Park, J.Y.; Cho, K.M.; Park, I.M. Effect of Mn addition on corrosion properties of biodegradable Mg-4Zn-0.5Ca-xMn alloys. *J. Alloys Compd.* **2017**, *695*, 1166–1174. [[CrossRef](#)]
16. Chen, H.; Yuan, B.; Zhao, R.; Yang, X.; Xiao, Z.; Aurora, A.; Iulia, B.A.; Zhu, X.; Iulian, A.V.; Zhang, X. Evaluation on the corrosion resistance, antibacterial property and osteogenic activity of biodegradable Mg-Ca and Mg-Ca-Zn-Ag alloys. *J. Magnes. Alloy.* **2021**, in press. [[CrossRef](#)]
17. Brar, H.S.; Wong, J.; Manuel, M.V. Investigation of the mechanical and degradation properties of Mg–Sr and Mg–Zn–Sr alloys for use as potential biodegradable implant materials. *J. Mech. Behav. Biomed. Mater.* **2012**, *7*, 87–95. [[CrossRef](#)] [[PubMed](#)]
18. Weng, W.; Biesiekierski, A.; Li, Y.; Dargusch, M.; Wen, C. A review of the physiological impact of rare earth elements and their uses in biomedical Mg alloys. *Acta Biomater.* **2021**, *130*, 80–97. [[CrossRef](#)] [[PubMed](#)]
19. Tsakiris, V.; Tardei, C.; Clicinschi, F.M. Biodegradable Mg alloys for orthopedic implants—A review. *J. Magnes. Alloy.* **2021**, in press. [[CrossRef](#)]
20. Pan, Y. Effect of calcium on the microstructure and corrosion behavior of microarc oxidized Mg-xCa alloys. *Biointerphases* **2018**, *13*, 011003. [[CrossRef](#)]
21. Kabir, H.; Munir, K.; Wen, C.E.; Li, Y.C. Recent research and progress of biodegradable zinc alloys and composites for biomedical applications: Biomechanical and biocorrosion perspectives. *Bioact. Mater.* **2021**, *6*, 836–879. [[CrossRef](#)]
22. Li, P.; Qian, J.Y.; Zhang, W.T.; Schille, C.; Schweizer, E.; Heiss, A.; Klotz, U.E.; Scheideler, L.; Wan, G.J.; Geis-Gerstorfer, J. Improved biodegradability of zinc and its alloys by sandblasting treatment. *Surf. Coat. Technol.* **2021**, *405*, 126678. [[CrossRef](#)]
23. Garcia-Mintegui, C.; Córdoba, L.C.; Buxadera-Palomero, J.; Marquina, A.; Jiménez-Piqué, E.; Ginebra, M.P.; Cortina, J.L.; Pegueroles, M. Zn-Mg and Zn-Cu alloys for stenting applications: From nanoscale mechanical characterization to in vitro degradation and biocompatibility. *Bioact. Mater.* **2021**, *6*, 4430–4446. [[CrossRef](#)]
24. Boehlert, C.J.; Knittel, K. The microstructure, tensile properties, and creep behavior of Mg-Zn alloys containing 0–4.4 wt.% Zn. *Mater. Sci. Eng. A* **2006**, *417*, 315–321. [[CrossRef](#)]
25. Farahany, S.; Bakhsheshi-Rad, H.R.; Idris, M.H.; Abdul Kadir, M.R.; Lotfabadi, A.F.; Ourdjini, A. In-situ thermal analysis and macroscopical characterization of Mg-xCa and Mg-0.5Ca-xZn alloy systems. *Thermochim. Acta* **2012**, *527*, 180–189. [[CrossRef](#)]
26. Jiang, W.; Cipriano, A.F.; Tian, Q.; Zhang, C.; Lopez, M.; Sallee, A.; Lin, A.; Cortez Alcaraz, M.C.; Wu, Y.; Zheng, Y.; et al. In vitro evaluation of MgSr and MgCaSr alloys via direct culture with bone marrow derived mesenchymal stem cells. *Acta Biomater.* **2018**, *72*, 407–423. [[CrossRef](#)]
27. Yin, P.; Li, N.F.; Lei, T.; Liu, L.; Ouyang, C. Effects of Ca on microstructure, mechanical and corrosion properties and biocompatibility of Mg-Zn-Ca alloys. *J. Mater. Sci. Mater. Med.* **2013**, *24*, 1365–1373. [[CrossRef](#)] [[PubMed](#)]
28. Min, Y.; Debaio, L.; Runfang, Z.; Minfang, C. Microstructure and properties of Mg-3Zn-0.2Ca alloy for biomedical application. *Rare Met. Mater. Eng.* **2018**, *47*, 0093–0098. [[CrossRef](#)]
29. Ding, P.; Liu, Y.; He, X.; Liu, D.; Chen, M. In vitro and in vivo biocompatibility of Mg–Zn–Ca alloy operative clip. *Bioact. Mater.* **2019**, *4*, 236–244. [[CrossRef](#)]
30. Zhang, E.; Yang, L. Microstructure, mechanical properties and bio-corrosion properties of Mg-Zn-Mn-Ca alloy for biomedical application. *Mater. Sci. Eng. A* **2008**, *497*, 111–118. [[CrossRef](#)]

31. Li, Y.C.; Li, M.H.; Hu, W.Y.; Hodgson, P.; Wen, C. Biodegradable Mg-Ca and Mg-Ca-Y alloys for Regenerative Medicine. *Mater. Sci. Forum* **2010**, *654–656*, 2192–2219. [[CrossRef](#)]
32. Zhang, C.; Lin, J.; Nguyen, N.T.; Guo, Y.; Xu, C.; Seo, C.; Villafana, E.; Jimenez, H.; Chai, Y.; Guan, R.; et al. Antimicrobial Bioresorbable Mg-Zn-Ca Alloy for Bone Repair in a Comparison Study with Mg-Zn-Sr Alloy and Pure Mg. *ACS Biomater. Sci. Eng.* **2020**, *6*, 517–538. [[CrossRef](#)]
33. Furukawa, M.; Horita, Z.; Nemoto, M.; Langdon, T.G. Review: Processing of metals by equal-channel angular pressing. *J. Mater. Sci.* **2001**, *36*, 2835–2843. [[CrossRef](#)]
34. Valiev, R.Z.; Langdon, T.G. Principles of equal-channel angular pressing as a processing tool for grain refinement. *Prog. Mater. Sci.* **2006**, *51*, 881–981. [[CrossRef](#)]
35. Rybalchenko, O.V.; Anisimova, N.Y.; Kiselevskiy, M.V.; Belyakov, A.N.; Tokar, A.A.; Terent'ev, V.F.; Prosvirnin, D.V.; Rybalchenko, G.V.; Raab, G.I.; Dobatkin, S.V. The influence of ultrafine-grained structure on the mechanical properties and biocompatibility of austenitic stainless steels. *J. Biomed. Mater. Res.* **2020**, *108*, 1460–1468. [[CrossRef](#)] [[PubMed](#)]
36. Bochvar, N.R.; Rybalchenko, O.V.; Tabachkova, N.Y.; Rybalchenko, G.V.; Leonova, N.P.; Rokhlin, L.L. Kinetics of phase precipitation in Al-Mg-Si alloys subjected to equal-channel angular pressing during subsequent heating. *J. Alloys Compd.* **2021**, *881*, 160583. [[CrossRef](#)]
37. Alawadhi, M.Y.; Sabbaghianrad, S.; Huang, Y.; Langdon, T.G. Evaluating the paradox of strength and ductility in ultrafine-grained oxygen-free copper processed by ECAP at room temperature. *Mater. Sci. Eng. A* **2021**, *802*, 140546. [[CrossRef](#)]
38. Martynenko, N.; Lukyanova, E.; Anisimova, N.; Kiselevskiy, M.; Serebryany, V.; Yurchenko, N.; Raab, G.; Birbilis, N.; Salishchev, G.; Dobatkin, S.; et al. Improving the property profile of a bioresorbable Mg-Y-Nd-Zr alloy by deformation treatments. *Materialia* **2020**, *13*, 100841. [[CrossRef](#)]
39. Estrin, Y.; Martynenko, N.; Anisimova, N.; Temralieva, D.; Kiselevskiy, M.; Serebryany, V.; Raab, G.; Straumal, B.; Wiese, B.; Willumeit-Römer, R.; et al. The effect of equal-channel angular pressing on the microstructure, the mechanical and corrosion properties, and the anti-tumor activity of magnesium alloyed with silver. *Materials* **2019**, *12*, 3832. [[CrossRef](#)]
40. Straumal, B.; Martynenko, N.; Temralieva, D.; Serebryany, V.; Tabachkova, N.; Shchetinin, I.; Anisimova, N.; Kiselevskiy, M.; Kolyanova, A.; Raab, G.; et al. The effect of equal-channel angular pressing on the microstructure, the mechanical properties, and biodegradation behavior of magnesium alloyed with Ag and Gd. *Crystals* **2020**, *10*, 918. [[CrossRef](#)]
41. Martynenko, N.; Lukyanova, E.; Serebryany, V.; Prosvirnin, D.; Terentiev, V.; Raab, G.; Dobatkin, S.; Estrin, Y. Effect of Equal Channel Angular Pressing on Structure, Texture, Mechanical and In-Service Properties of a Biodegradable Magnesium Alloy. *Mater. Lett.* **2019**, *238*, 218–221. [[CrossRef](#)]
42. ASTM. *ASTM G59–97(2003) Standard Test Method for Conducting Potentiodynamic Polarization Resistance Measurements*; ASTM International: West Conshohocken, PA, USA, 2006.
43. ASTM. *ASTM G31–21, Standard Guide for Laboratory Immersion Corrosion Testing of Metals*; ASTM International: West Conshohocken, PA, USA, 2004.
44. Choudhary, R.; Venkatraman, S.K.; Bulygina, I.; Senatov, F.; Kaloshkin, S.; Anisimova, N.; Kiselevskiy, M.; Knyazeva, M.; Kukui, D.; Walther, F.; et al. Biomineralization, dissolution and cellular studies of silicate bioceramics prepared from eggshell and rice husk. *Mater. Sci. Eng. C* **2021**, *118*, 111456. [[CrossRef](#)]
45. Zimina, A.; Senatov, F.; Choudhary, R.; Kolesnikov, E.; Anisimova, N.; Kiselevskiy, M.; Orlova, P.; Strukova, N.; Generalova, M.; Manskikh, V.; et al. Biocompatibility and Physico-Chemical Properties of Highly Porous PLA/HA Scaffolds for Bone Reconstruction. *Polymers* **2020**, *12*, 2938. [[CrossRef](#)] [[PubMed](#)]
46. Persaud-Sharma, D.; McGoron, A. Biodegradable Magnesium Alloys: A Review of Material Development and Applications. *J. Biomim Biomater. Tissue Eng.* **2012**, *12*, 25–39. [[CrossRef](#)]
47. Rodríguez-Hernández, C.O.; Torres-García, S.E.; Olvera-Sandoval, C.; Ramírez-Castillo, F.Y.; Muro, A.L.; Avelar-Gonzalez, F.J.; Guerrero-Barrera, A.L. Cell culture: History, development and prospects. *Int. J. Curr. Res. Aca Rev.* **2014**, *2*, 188–200.
48. Li, Z.; Gua, X.; Lou, S.; Zheng, Y. The development of binary Mg–Ca alloys for use as biodegradable materials within bone. *Biomater.* **2008**, *29*, 1329–1344. [[CrossRef](#)] [[PubMed](#)]
49. Anvari-Yazdi, A.F.; Tahermanesh, K.; Hadavi, S.M.M.; Taleai-Khozani, T.; Razmkhah, M.; Abed, S.M.; Mohtasebi, M.S. Cytotoxicity assessment of adipose-derived mesenchymal stem cells on synthesized biodegradable Mg-Zn-Ca alloys. *Mater. Sci. Eng. C* **2016**, *69*, 584–597. [[CrossRef](#)]
50. Jiang, P.; Blawert, C.; Zheludkevich, M.L. The Corrosion Performance and Mechanical Properties of Mg-Zn Based Alloys—A Review. *Corros. Mater. Degrad.* **2020**, *1*, 92–158. [[CrossRef](#)]
51. Salahshoor, M.; Guo, Y. Biodegradable orthopedic magnesium-calcium (MgCa) alloys, processing, and corrosion performance. *Materials* **2012**, *5*, 135–155. [[CrossRef](#)]
52. Wu, G.; Ibrahim, J.M.; Chu, P.K. Surface design of biodegradable magnesium alloys—A review. *Surf. Coat. Technol.* **2013**, *233*, 2–12. [[CrossRef](#)]
53. Nakamura, S.; Matsumoto, T.; Sasaki, J.-I.; Egusa, H.; Lee, K.Y.; Nakano, T.; Sohmura, T.; Nakahira, A. Effect of Calcium Ion Concentrations on Osteogenic Differentiation and Hematopoietic Stem Cell Niche-Related Protein Expression in Osteoblasts. *Tissue Eng. Part A* **2010**, *16*, 2467–2473. [[CrossRef](#)]
54. Makkar, P.; Sarkar, S.K.; Padalhin, A.R.; Moon, B.-G.; Lee, Y.S.; Lee, B.T. In vitro and in vivo assessment of biomedical Mg–Ca alloys for bone implant applications. *J. Appl. Biomater. Funct.* **2018**, *16*, 126–136. [[CrossRef](#)]

55. Zhang, N.; Zhao, D.; Liu, N.; Wu, Y.; Yang, J.; Wang, Y.; Xie, H.; Ji, Y.; Zhou, C.; Zhuang, J.; et al. Assessment of the degradation rates and effectiveness of different coated Mg-Zn-Ca alloy scaffolds for in vivo repair of critical-size bone defects. *J. Mater. Sci. Mater. Med.* **2018**, *29*, 138. [[CrossRef](#)] [[PubMed](#)]
56. Galow, A.-M.; Rebl, A.; Koczan, D.; Bonk, S.M.; Baumann, W.; Gimsa, J. Increased osteoblast viability at alkaline pH in vitro provides a new perspective on bone regeneration. *Biochem. Biophys.* **2017**, *10*, 17–25. [[CrossRef](#)]
57. Wong, C.-C.; Wong, P.-C.; Tsai, P.-H.; Jang, J.S.-C.; Cheng, C.-K.; Chen, H.-H.; Chen, C.-H. Biocompatibility and Osteogenic Capacity of Mg-Zn-Ca Bulk Metallic Glass for Rabbit Tendon-Bone Interference Fixation. *Int. J. Mol. Sci.* **2019**, *20*, 2191. [[CrossRef](#)] [[PubMed](#)]
58. Sollazzo, V.; Lucchese, A.; Palmieri, A.; Carnevali, G.; Iaccarino, C.; Zollino, I.; Della Valle, M.; Pezzetti, F.; Brunelli, G.; Carinci, F. Calcium sulfate stimulates pulp stem cells towards osteoblasts differentiation. *Int. J. Immunopathol. Pharmacol.* **2011**, *24* (Suppl. 2), 51–57. [[CrossRef](#)] [[PubMed](#)]
59. Müller, P.; Bulnheim, U.; Diener, A.; Lüthen, F.; Teller, M.; Klinkenberg, E.-D.; Neumann, H.-G.; Nebe, B.; Liebold, A.; Steinhoff, G.; et al. Calcium phosphate surfaces promote osteogenic differentiation of mesenchymal stem cells. *J. Cell. Mol. Med.* **2008**, *12*, 281–291. [[CrossRef](#)] [[PubMed](#)]
60. Goldberg, M.A.; Krohicheva, P.A.; Fomin, A.S.; Khairutdinova, D.R.; Antonova, O.S.; Baikin, A.S.; Smirnov, V.V.; Fomina, A.A.; Leonov, A.V.; Mikheev, I.V.; et al. In situ magnesium calcium phosphate cements formation: From one pot powders precursors synthesis to in vitro investigations. *Bioact. Mater.* **2020**, *5*, 644–658. [[CrossRef](#)]
61. Sathayaraj, M.K.R.; Narayanan, S. Controlling the rate of degradation of Mg using magnesium fluoride and magnesium fluoride-magnesium phosphate duplex coatings. *J. Magnes. Alloy.* **2021**, in press. [[CrossRef](#)]